The Journal of Adhesion

ISSN: 0021-8464 (Print) 1545-5823 (Online) Journal homepage: www.tandfonline.com/journals/gadh20

Cyclic creep response of adhesively bonded steel lap joints

P. N. B. Reis, A. M. Pereira, J. A. M. Ferreira & J. D. M. Costa

To cite this article: P. N. B. Reis, A. M. Pereira, J. A. M. Ferreira & J. D. M. Costa (2017) Cyclic creep response of adhesively bonded steel lap joints, The Journal of Adhesion, 93:9, 704-715, DOI: 10.1080/00218464.2016.1146880

To link to this article: https://doi.org/10.1080/00218464.2016.1146880

THE JOURNAL OF ADHESION
2017, VOL. 93, NO. 9, 704–715
http://dx.doi.org/10.1080/00218464.2016.1146880

Taylor & Francis
Taylor & Francis Group

Cyclic creep response of adhesively bonded steel lap joints

P. N. B. Reis[a], A. M. Pereira [b], J. A. M. Ferreira[c], and J. D. M. Costa[c]

[a]Deptartment of Electromechanical Engineering, University of Beira Interior, Covilhã, Portugal; [b]ESTG/CDRsp, Polytechnic Institute of Leiria, Leiria, Portugal; [c]CEMUC, Department of Mechanical Engineering, University of Coimbra, Coimbra, Portugal

ABSTRACT

The viscoelastic nature of polymeric adhesives means that the effect of fatigue frequency has to be treated cautiously. However, this subject has received limited attention and very few studies can be found. Therefore, this work aims at investigating the cyclic creep response of adhesively bonded steel lap joints. Load-controlled fatigue tests were performed with shear stresses of 9.1, 7.4, and 6.3 MPa, which are typically low cycle fatigue stresses. Only during the last 20% of fatigue life can we observe an increase in the cycle hysteresis area due to the decrease of the shear stiffness caused by the failure mechanisms. Under fatigue load, the maximum/minimum strain curves exhibit a shape being similar to that of the steady creep curves, in which occurs a second stage with nearly constant strain rate, independently of the number of cycles and increasing with the load range. A linear relationship between the log cyclic creep rate and the log of the number of cycles to failure was observed, indicating that fatigue behaviour is strictly related to cyclic creep.

ARTICLE HISTORY
Received 24 November 2015
Accepted 14 January 2016

KEYWORDS
Creep; epoxy/epoxides; fatigue; lap joints; steels

1. Introduction

The use of adhesive joints is becoming increasingly important in aerospace, automotive, and other industries where traditional fasteners are discouraged [1]. In fact, adhesive bonding distributes stresses over the whole bonded region, which promotes lower stress concentrations than the conventional fastening techniques (bolted, riveted, or welded). However, for the industries mentioned above, adhesive joints are usually subjected to complex fatigue load histories characterized by changes in the amplitude, stress ratio (R), frequency, and waveform of the cycling stresses.

Several studies report that the fatigue strength of adhesive joints, for example, is highly dependent on the stress ratio (R) [2–7] and frequency of the cyclic stresses [7–11]. However, if the time taken to generate fatigue data is responsible for relatively high frequencies, normally between 5 and 10 Hz [12], literature reports that the frequency effects on the fatigue life should be considered as

CONTACT P. N. B. Reis preis@ubi.pt Department of Electromechanical Engineering, University of Beira Interior, Calçada, Fonte do Lameiro, Edifício I das Engenharias 6201-001, Covilhã, Portugal.

Color versions of one or more figures in this article can be found online at www.tandfonline.com/gadh.

consequence of the viscoelastic nature of polymeric adhesives. On the other hand, the frequency effects show to be sensitive to the different adhesive systems [12,13].

According to Pirondi and Nicoletto [9] and Ashcroft et al. [14], when the adhesives exhibit strong viscoelastic behaviour, the influence of loading frequency is markedly temperature dependent. Therefore, in this case, the frequency effect should be discussed in terms of temperature, especially for adhesives where the mechanical properties are markedly temperature dependent [9]. On other hand, studies developed by Althof [15] show that the fatigue failure is creep-controlled at low frequencies, provided that no significant change of temperature occurs. Marceau et al. [16] found that, in lap-shear and double cantilever beam (DCB) joints, low-frequency fatigue was more damaging to adhesive joints than high-frequency fatigue. According to Reis et al. [11], for the higher shear stress amplitudes, the frequency presents only a marginal effect, since fatigue lives are very similar for the different frequencies. On the other hand, for the lower shear stress amplitudes, the fatigue life of the adhesive joints is highly dependent on the frequency. The fatigue tests performed at 2 Hz promotes the smallest fatigue lives, while the higher fatigue lives were obtained for the frequency level of 10 Hz. Above 10 Hz, the fatigue life decreases but with higher values than the ones observed for 2 Hz. The results were explained by the predominance of the creep mechanism at 2 Hz and by the temperature at 40 Hz.

In this context, this work aims at investigating the cyclic creep response of adhesively bonded steel lap joints. For this purpose, S–N diagrams under constant amplitude fatigue tests are obtained at 2 Hz. The maximum and minimum strain values plotted against the number of cycles and the cyclic creep rate against number of cycles for the different values of σ_{max} are analysed.

2. Materials and experimental procedure

Docol 1000 DP high elastic limit steel plates (supplied by SSAB, Borlänge, Sweden) with 1.5 mm thickness were used as material for the adherends of the double strap joints studied. Tensile tests were performed according with ASTM E8/E8M-09 [17], in order to characterize the adherends, and the main mechanical properties can be found in Table 1. Typical stress–strain curves are shown in Fig. 1.

Table 1. Mechanical properties of the Adhesive and Adherends.

Material	σ_{UTS} (MPa)	σ_{YS} (MPa) Strain 0.2%	E (GPa)
Adhesive (Araldite® 420 A/B)	35	27	1.85
Docol 1000 High-strength steel	1018 (15)	782 (16)	201 (11)

() Standard deviation.

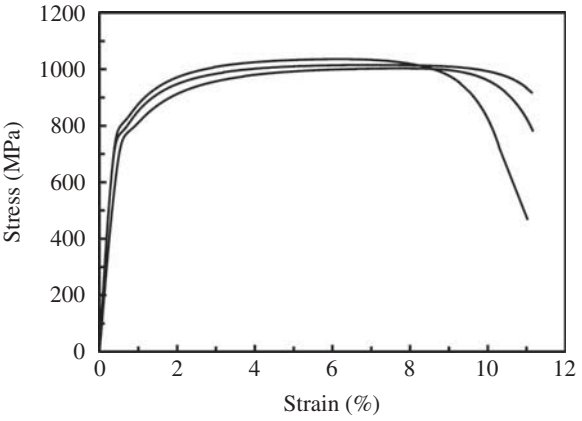

Figure 1. Stress versus strain curves obtained from tensile tests to characterize the adherends (Docol 1000 DP).

The specimens were manufactured as 10-mm-wide bars cut from the plates and bonded with "Araldite® 420 A/B" adhesive epoxy (Huntsman Advanced Materials, Everberg, Belgium). The main properties of the adhesive can be found in Table 1, and they were obtained from the literature [18]. The geometry and dimensions of the specimens are shown in Fig. 2. Abrasive polishing with silicon carbide paper type P220 (R_z = 4.66 ± 0.34 μm) was used and, finally, the surface was cleaned with dry air and alcohol. In order to ensure a constant bondline thickness, the specimens were compressed with a constant pressure of about 0.12 MPa, uniformly applied during all cure time, as suggested in previous works developed by the authors [19,20]. The bondline thickness was measured after tests using surface roughness topography station (Mahr) equipped with a laser sensor (Rodenstock RM 600-S) [20]. An average value of 63 μm was obtained without significant dispersion.

For this adhesive, as suggested by the supplier [21], the cure procedure occurred during 4 h at 50°C. However, in terms of mechanical properties, the open literature reports benefits when a post-cure is performed [22–24]. To verify its effect on the fatigue strength, S–N curves were compared between specimens exposed to a post-cure of 6 h at 30°C and other ones exposed to a post-cure of 24 h at 30°C.

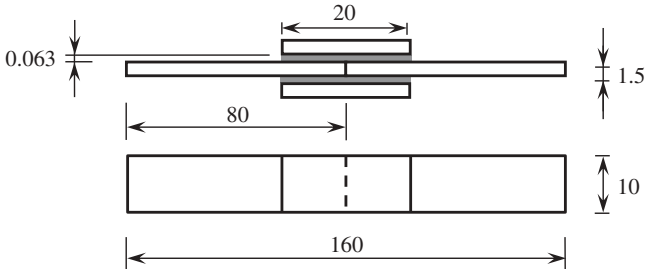

Figure 2. Specimen geometry with dimensions in mm.

Constant amplitude loading fatigue tests were carried out in tension using a servohydraulic machine (Instron model 1341), equipped with a 100 kN load cell and controlled by a computer with data acquisition. Tests were performed at room temperature, under constant amplitude sinusoidal waveform loading, a stress ratio of R=0.05 and a frequency of 2 Hz. The displacement between upper and lower specimen parts was measured using an axial extensometer Instron, Model 2620-601. Figure 3 shows the specimen clamping grips and the extensometer coupled to the specimen. Along the present study, the tests were replicated four times for each loading level and the total separation of the specimens was adopted as the failure criterion.

Previously, tensile tests were performed using an electromechanical machine (Instron model 4206) to obtain the static shear strength. Five tests were carried out at room temperature and an average around 10.1 MPa was obtained with a standard deviation of 0.35 MPa. The shear stresses used during the fatigue tests were 9.1, 7.4, and 6.3 MPa. They represent, respectively, 90.1%, 73.3%, and 62.4% of the ultimate strength. According to the literature, these values are greater than 50% of the ultimate shear strength and, in this context, they are typically low-cycle fatigue (LCF) stresses [25]. This is relevant for the present study, because high LCF stresses promote large strains. Moreover, it was expected that the experimental tests were carried out at constant strain rate. However, as the tests were performed at constant frequency, the shear strain rate ranged between 0.544 and 0.713 μstrain/s, for maximum shear stresses of 6.3 and 9.1 MPa, respectively. In this case, these values are so close that a significant influence on the cyclic creep response is not predictable.

Figure 3. Experimental setting showing the specimen clamping grips and the extensometer coupled to the specimen.

3. Results and discussion

S–N diagram, representing the fatigue life dependence on stress, is the main tool used to analyse fatigue test results based on the stress-life approach [26]. The results of fatigue tests for the different maximum shear stresses studied (9.1, 7.4, and 6.3 MPa) are presented in Fig. 4, in terms of maximum shear stress versus number of cycles to failure. The effect of the post-cure time is also shown in Fig. 4. Mean S–N curves, fitted to the experimental results by least squares method, are also superimposed in Fig. 4.

It is possible to observe the benefits of the post-cure during 24 hours, promoting an average fatigue life around 4.8 times higher than that occurred for 6 hours. These results present the same tendency that is observed in static tests, where the post-cure promoted benefits in terms of tensile strength [22–24]. Therefore, the following fatigue and cyclic creep analyses will be performed only for the samples exposed to a post-cure of 24 h at 30°C.

Figure 5 shows the typical damage morphology observed after the fatigue tests, relatively to the samples exposed, which is in good agreement with the

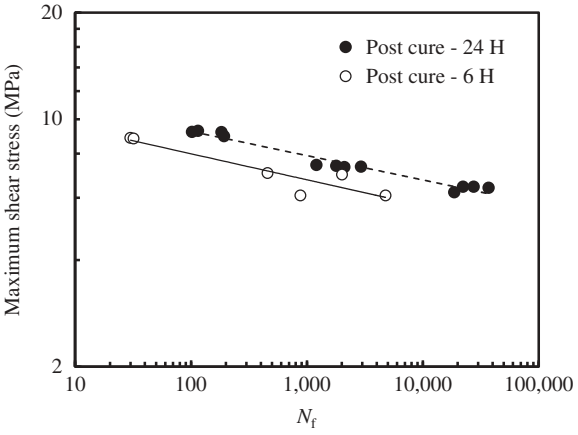

Figure 4. Constant maximum shear stress versus number of cycles to failure.

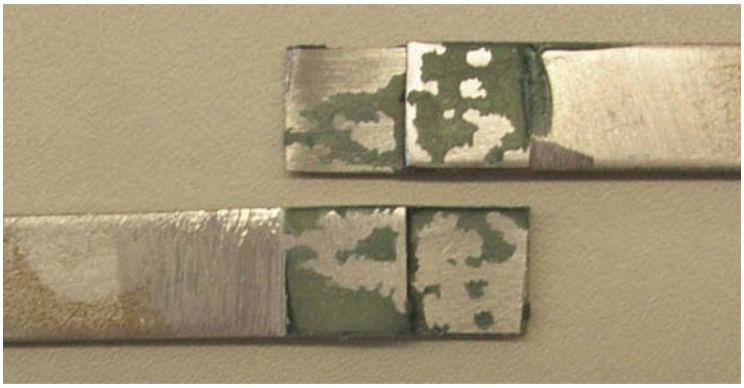

Figure 5. Typical failure surfaces for samples with post-cure of 24 h at 30°C.

literature [6,11,24]. In a previous study performed by the authors, using similar specimens, no adhesive film left on the adhesive/adherend interface was observed [11]. Therefore, it is possible to conclude that an adhesive failure occurs according to ASTM D 5573-99 [27]. Debonding typically initiates at the edge of the patches, where the stress concentration and peel stresses are highest, and proceeds towards the centre of the path [28–30], although higher values of both stiffness and elastic limit of the adherends promote a more uniform distribution of shear stresses in the adhesive [31].

Figure 6 shows the typical evolution of the load–displacement hysteresis loops during the fatigue tests. It is possible to conclude that the load–displacement curves under loading and unloading branches are nonlinear. For all tests it was observed that the cycle hysteresis loops are very similar on the first 80% of the fatigue life and, only on the remaining fatigue life, it is observed both a slope change and an increase of the cycle hysteresis area.

Literature reports that an increase of the cycle hysteresis area is a consequence of the material cyclic softening [32]. In this case, the strain softening is often caused by the nucleation and growth of microvoids inside the materials. Therefore, for the shear stress levels applied in the fatigue tests, a cohesive failure in the epoxy adhesive would be expectable as consequence of the nucleation and growth of microvoids. However, as shown in Fig. 5, an adhesive failure was observed, and the cyclic softening can be related with the nucleation and growth of adhesive/adherend debonding.

Figure 7 shows the shear strain (γ) against number of cycles (N). Shear strain (γ) is defined by Equation (1):

$$\gamma = \frac{\mathrm{d}u}{\mathrm{d}v} \tag{1}$$

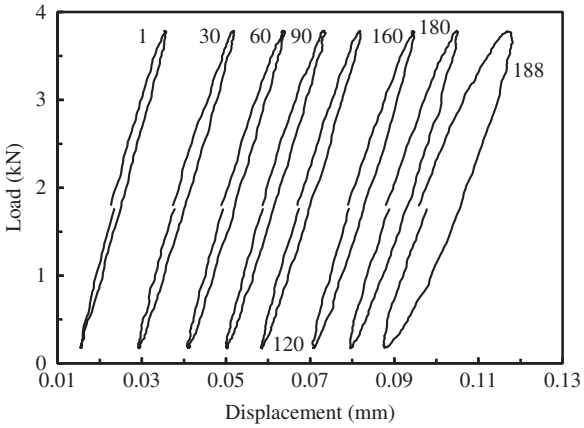

Figure 6. Typical evolution of the hysteresis cycles obtained over a test performed at maximum shear stress of 9.1 MPa. Samples with post-cure of 24 h at 30°C.

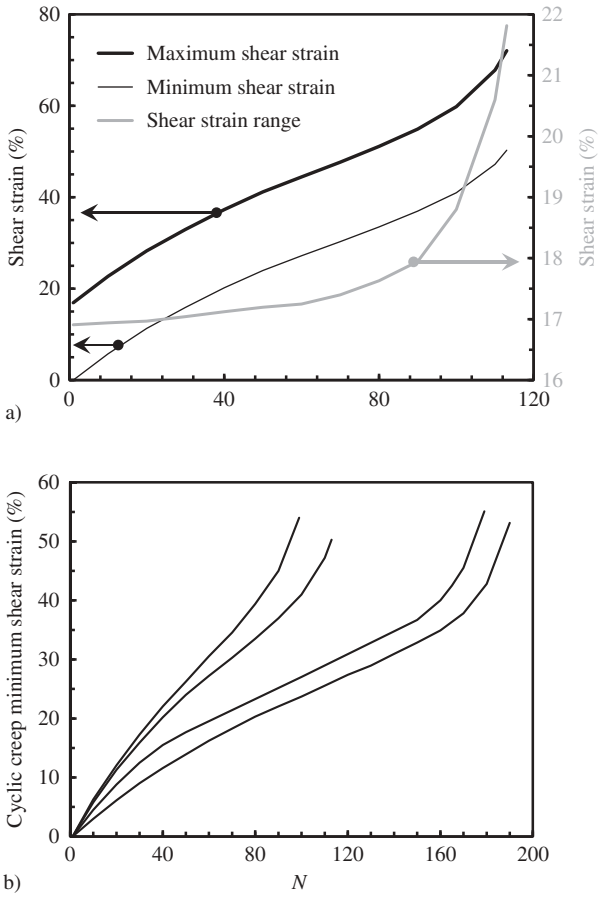

Figure 7. Shear strain (γ) versus number of cycles (N) in terms of: (a) maximum and minimum values for a maximum shear stress of 9.1 MPa; (b) cyclic creep minimum shear strain for all tests performed at maximum shear stress of 9.1 MPa. Samples with post-cure of 24 h at 30°C.

where du and dv are the infinitesimal axial and transverse displacement, respectively. Taking into account the higher stiffness of the adherends, an approximate value for the shear strain (γ) can be calculated by Equation (2):

$$\gamma \approx \frac{\delta/2}{t} \tag{2}$$

where δ is the axial displacement measured by the axial extensometer and t is equal to the bondline thickness (0.063 mm). In Equation (2), the axial displacement (δ) is divided by 2 because it corresponds to the contribution of the two central adherends.

Representative curves of γ versus N, obtained for a maximum shear stress of 9.1 MPa, are shown in Fig. 7(a)), where the maximum and minimum shear strain values, γ_{max} and γ_{min}, respectively, are plotted against the number of cycles (N). The minimum shear strain, γ_{min}, represents the cyclic

creep shear strain, while the maximum shear strain, γ_{max}, represents the summation of the cyclic creep shear strain with the elastic strain. The shear strain range, $\Delta\gamma = \gamma_{max} - \gamma_{min}$, is also shown in Fig. 7(a), using an amplified secondary scale for clarity, where the variation of the shear stiffness along the test is shown (because the tests were performed at constant amplitude loading). Figure 7(b) shows all shear strain curves, in terms of minimum values, obtained for a maximum shear stress of 9.1 MPa. It is possible to observe a significant variation of fatigue life, as can also be observed in Fig. 4. A similar dispersion of fatigue lives was also observed for the other maximum shear stresses.

The minimum and maximum shear strain curves shown in Fig. 7 present a similar shape of the steady creep curves (i.e., creep under constant applied stress), which are characterized by an initial stage with a rapid increase of strain, followed by a second stage with constant strain rate and a third stage with an abrupt strain increase before the final fracture [32–34]. On the other hand, the curve $\Delta\gamma$ versus N presents only the second and third stages. In terms of second stage, the shear strain range is almost constant with the number of cycles, and the variation of the shear strain range with the number of cycles $d(\Delta\gamma)/dN$ is about 61 μstain/cycle. Finally, in the third stage, $d(\Delta\gamma)/dN$ has a fast growth with the number of cycles due to the decrease of the shear stiffness caused by the failure mechanisms. Consequently, the area of the cycle hysteresis loops increases as shown in Fig. 6.

Figure 8 compares representative curves obtained for 6.3, 7.4, and 9.1 MPa stress levels, showing the cyclic creep shear strain (γ_{min}) against the number of cycles (N). The x-axis was represented in logarithmic scale, in order to increase the clarity of the figure. As expected, higher loads promote lower lives and higher final strain values, in agreement with studies developed by

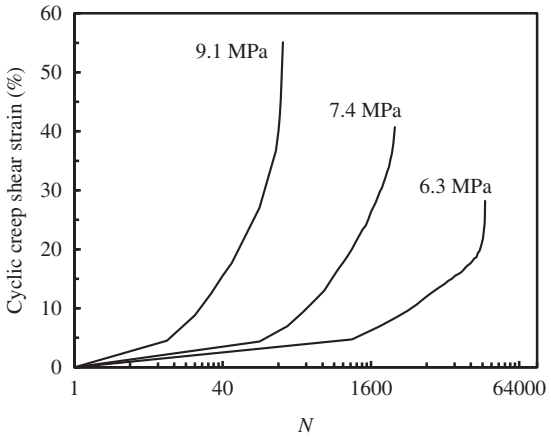

Figure 8. Comparison between three cyclic creep shear strain curves (γ_{min}) versus number of cycles (N), obtained for maximum shear stresses of 6.3, 7.4, and 9.1 MPa. Samples with post-cure of 24 h at 30°C.

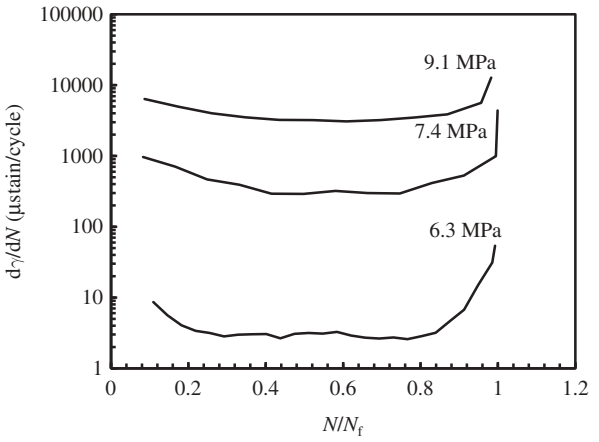

Figure 9. Cyclic creep shear strain rate (dγ/dN) against normalised number of cycles. Samples with post-cure of 24 h at 30°C.

Bai and Wang [32] in a polymeric material. However, other studies [33–35] show that higher loads promote lower final strain values. This disagreement can be explained by the different damage mechanisms involved in the creep behaviour of composite materials and adhesive joints.

To understand better the behaviour reported in Fig. 8, the cyclic creep shear strain rate ($d\gamma_{min}/dN$) against the normalised number of cycles to failure (N/N_f) is plotted in Fig. 9. Representative curves of each stress level are presented, where N is the current number of cycles and N_f the number of cycles to failure. All curves exhibit a nearly constant second stage, whereas the cyclic creep rate proves to be highly dependent on the shear stress. For the lowest shear stresses (6.3 MPa), the cyclic creep rate is about 3 μstain/cycle, whereas for shear stresses of 7.4 and 9.1 MPa, the cyclic creep rate is around 300 and 3,200 μstain/cycle, respectively.

According to Bernasconi and Kulin [35], when a linear relationship is observed between the log(cyclic creep rate) and the log(number of cycles to failure), the fatigue behaviour is strictly dependent of the cyclic creep rate, taking into account the normal linear relationship between the log(applied maximum stress) and log(N_f). Figure 10 shows the log ($d\gamma_{min}/dN$) versus log (N_f), where the cyclic creep rate was obtained by the second stage slope of the $\gamma_{min} - N$ curve with a correlation coefficient higher than 0.95 for all tests. All data fell on the same line as observed by the previous authors, suggesting that fatigue behaviour is strictly related to cyclic creep, despite the data being obtained only for the frequency of 2 Hz.

Finally, the evolution of the cyclic creep rate ($d\gamma_{min}/dN$) with the maximum shear stress is shown in Fig. 11. As expected, it is possible to observe that the cyclic creep rate increases with the increasing of the shear stress. In spite of the data scatter, the results are reasonably fitted by Equation (2):

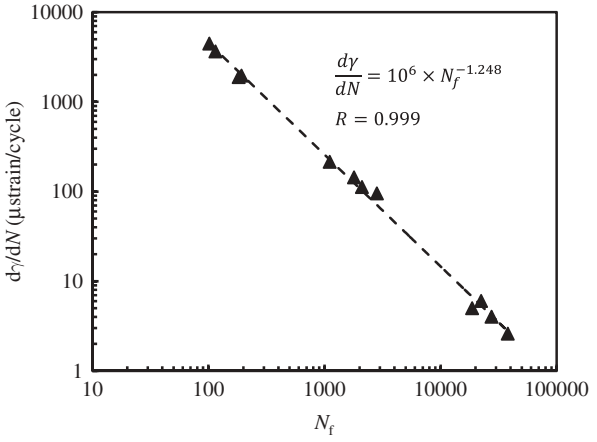

Figure 10. Cyclic creep rate (dγ/dN) against number of cycles to failure. Samples with post-cure of 24 h at 30°C.

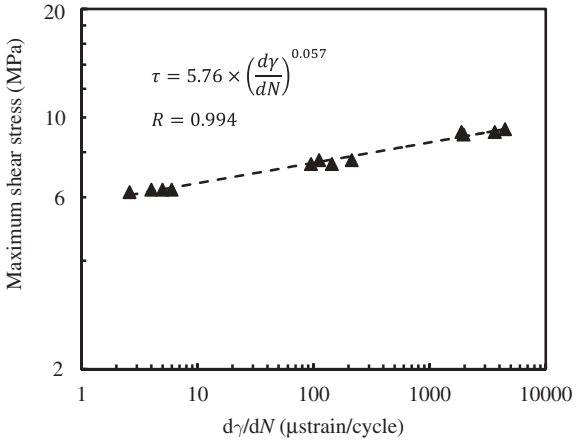

Figure 11. Maximum shear stress versus cyclic creep rate (dγ/dN). Samples with post-cure of 24 h at 30°C.

$$\tau = 5.76\left(\frac{\mathrm{d}\gamma}{\mathrm{d}N}\right)^{0.057} \tag{2}$$

with a correlation coefficient of 0.994. The linear relationships between cyclic creep strain rate versus both N_f and shear stress curves, in double logarithmic scales, confirm that fatigue behaviour is strictly related to cyclic creep.

4. Conclusions

This study investigated the cyclic creep response of adhesively bonded steel lap joints. Increasing the post-cure period from 6 hours to 24 hours promotes an increase on fatigue life around 4.8 times. It has been proved that the

fatigue behaviour, for the frequency level studied, is strictly related to cyclic creep rate. This conclusion was supported by the linear relationship observed between the log(cyclic creep rate) with both log(number of cycles to failure) and shear stress curves. The cyclic creep shear strain rate versus the normalised number of cycles to failure showed a second stage almost constant and very dependent of the shear stress. Finally, the minimum and maximum shear strain curves can be characterized by three stages, similar to those observed for creep under constant applied stress, opposite to the shear strain range curves, where there are only two stages. The decrease of the shear stiffness caused by the failure mechanisms is responsible for the higher area of the cycle hysteresis loops observed.

ORCID

A. M. Pereira http://orcid.org/0000-0003-1219-0596

References

[1] Loureiro, A. L., da Silva, L. F. M., Sato, C., and Figueiredo, M. A. V., *J. Adhes.* **86**, 765–787 (2010).
[2] Underhill, P. R. and DuQuesnay, D. L., *Int. J. Adhes. Adhes.* **26**, 62–66 (2006).
[3] Gomatam, R. R. and Sancaktar, E., *J. Adhes. Sci. Technol.* **20**, 69–86 (2006).
[4] Crocombe, A. D. and Richardson, G., *Int. J. Adhes. Adhes.* **19**, 19–27 (1999).
[5] Kwofie, S., *Int. J. Fatigue* **23**, 829–836 (2001).
[6] Pereira, A. M., Reis, P. N. B., and Ferreira, J. A. M., *J. Adhes.* doi:10.1080/00218464.2015.1110699.
[7] Gomatam, R. R. and Sancaktar, E., *J. Adhes. Sci. Technol.* **20**, 53–68 (2006).
[8] Luckyram, J. and Vardy, A. E., *J. Adhes.* **26**, 273–291 (1988).
[9] Pirondi, A. and Nicoletto, G., *Eng. Fract. Mech.* **71**, 859–871 (2004).
[10] Al-Ghamdi, A. H., Ashcroft, I. A., Crocombe, A. D., and Wahab, M. M. A., *J. Adhes.* **79**, 1161–1182 (2003).
[11] Reis, P. N. B., Monteiro, J. F. R., Pereira. A. M., Ferreira, J. A. M., and Costa, J. D. M., *Int. J. Adhes. Adhes.* **63**, 66–73 (2015).
[12] Luckyram, J. and Vardy, A. E., *J. Adhes.* **26**, 273–291 (1988).
[13] Mostovoy, S. and Ripling, E. J., *Adhesion Science and Technology*, (Plenum Press, New York, 1975), Vol. 9, pp. 64–80.
[14] Ashcroft, I. A., Hughes, D. J., Shaw, S. J., Abdel Wahab, M., and Crocombe, A., *J. Adhes.* **75**, 61–88 (2001).
[15] Althof, W., *Proc. of the Int. Symp. on "Adhesive Joints: Formation, Characteristics and Testing"*, Ed. Mittal, K. L., (Plenum Press, New York, 1984), pp. 659–677.
[16] Marceau, J. A., McMillan, J. C., and Scardino, W. M., *Proc. of the 22nd National SAMPE Symposium and Exhibition*, San Diego, California (1977), pp. 64–80.
[17] ASTM E8/E8M-11. Standard test methods for tension testing of metallic materials. *Annual Book of ASTM Standards*, 03.01 (2013).

[18]
Braga, D. F. O., de Sousa, L. M. C., Infante, V., da Silva, L. F. M., and Moreira, P. M. G. P., *J. Adhes*. doi:10.1080/00218464.2015.1085860.
[19] Pereira, A. M., Ferreira, J. A. M., Antunes, F. V., and Bártolo, P. J., *J. Mater. Process. Technol*. **210**, 610–617 (2010).
[20] Reis, P. N. B., Ferreira, J. A. M., and Richardson M. O. W., *J. Thermoplast. Compos. Mater*. **25**, 3–13 (2012).
[21] Araldites 420 A/B. Aerospace, parts manufacturing and repair, selector guide. *Edited by Hunstman Advanced Materials*, (GmbH, Switzerland, 2007).
[22] Cognard, J. Y., Créac'Hcadec, R., da Silva, L. F. M., Teixeira, F. G., Davies, P., and Peleau, M., *J. Adhes*. **87**, 804–825 (2011).
[23] Cognard, J. Y., Créac'hcadec, R., Maurice, J., Davies, P., Peleau, M., and da Silva, L. F. M., *J. Adhes. Sci. Technol*. **24**, 1977–1994 (2010).
[24] Pereira, A. M., Reis, P. N. B., Ferreira, J. A. M., and Antunes, F. V., *Int. J. Adhes. Adhes*. **47**, 99–104 (2013).
[25] Harik, V. M., Klinger, J. R., and Bogetti, T. A., *Int. J. Fatigue* **24**, 455–462 (2002).
[26] Casas-Rodriguez, J. P., Ashcroft, I. A., and Silberschmidt, V. V., *J. Sound Vib*. **308**, 467–478 (2007).
[27] ASTM D 5573-99. Standard practice for classifying failure modes in fiber-reinforced-plastic (FRP) joints. *Annual Book of ASTM Standards*, 15.03, 2002.
[28] Hart-Smith, L. J., *ASTM STP* **876**, 238–266 (1985).
[29] Pandey, P. C., Shankaragouda, H., and Singh, A. K., *Comput. Struct*. **70**, 387–413 (1999).
[30] Reis, P. N. B., Antunes, F. J. V., and Ferreira, J. A. M., *Compos. Struct*. **67**, 125–133 (2005).
[31] Reis, P. N. B., Ferreira, J. A. M., and Antunes, F., *Int. J. Adhes. Adhes*. **31**, 193–201 (2011).
[32] Bai, S.-L. and Wang, M., *Polymer* **44**, 6537–6547 (2003).
[33] Ferreira, J. A. M., Reis, P. N. B., and Costa, J. D. M., *Int. J. Fatigue* **18**, 227–233 (1996).
[34] Ferreira, J. A. M., Reis, P. N., Costa, J. D. M., and Richardson, M. O. W., *Compos. Sci. Technol*. **62**, 1373–1379 (2002).
[35] Bernasconi, A. and Kulin, R. M., *Polym. Compos*. **30**, 154–161 (2009).